**Inventory of Supplemental information:**

Supplemental Figures 1-7:

**Inventory of Supplemental information:**

Supplemental Figures 1-7:

Supplemental Figure 1, related to Figure 1.

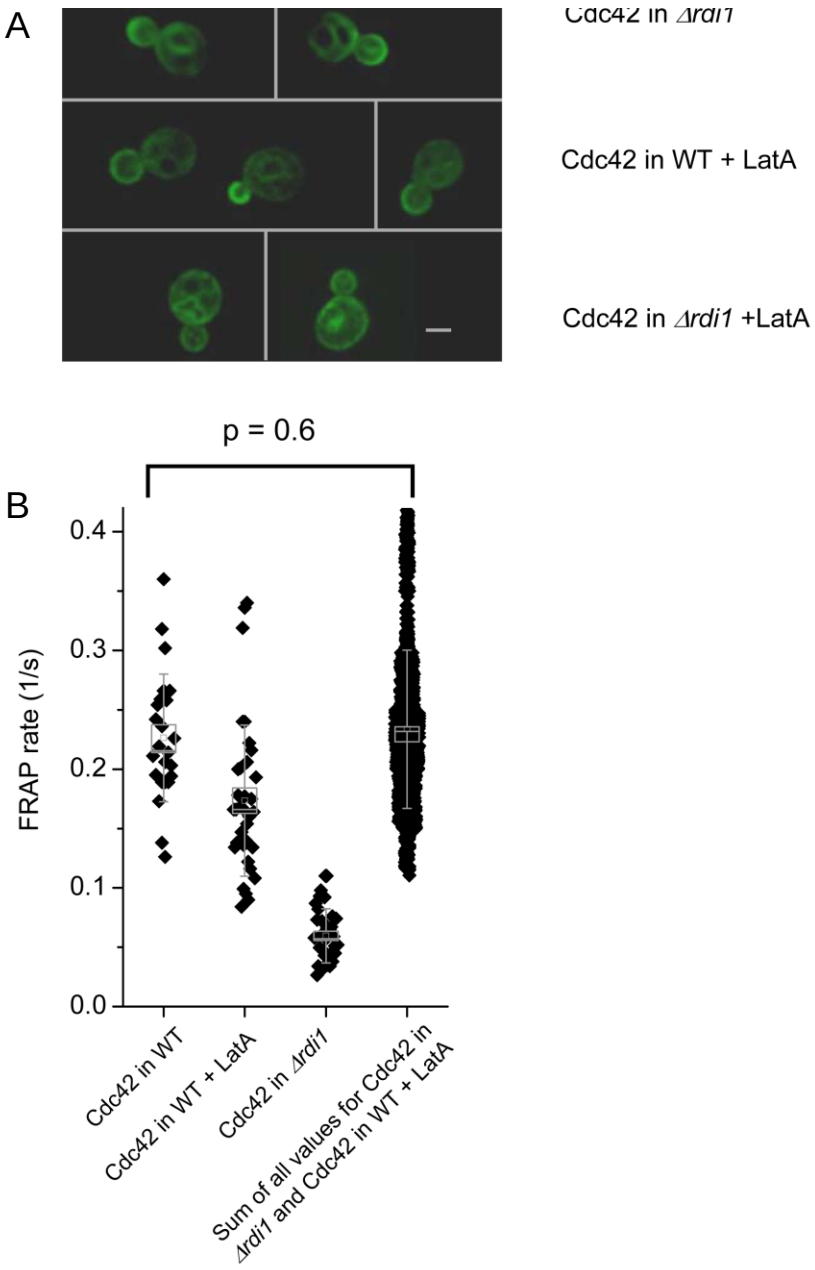

Supplemental Figure 2, related to Figure 2.

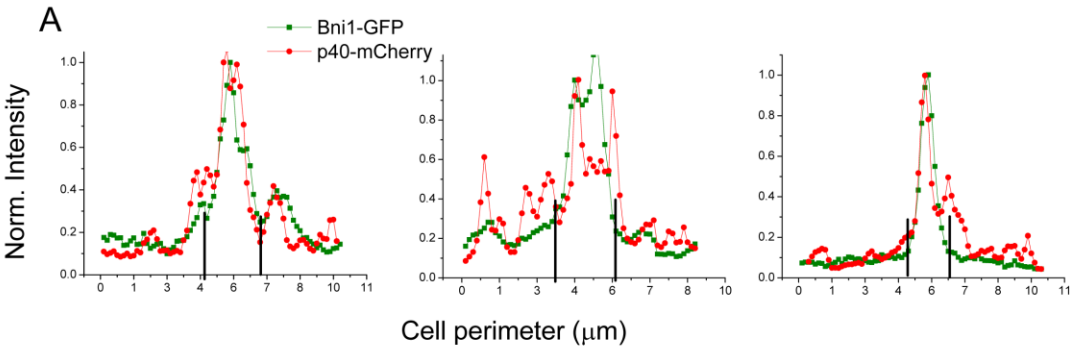


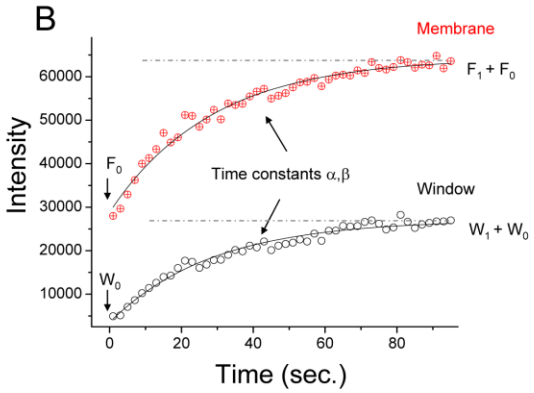

Supplemental Figure 3, related to Figure 3.

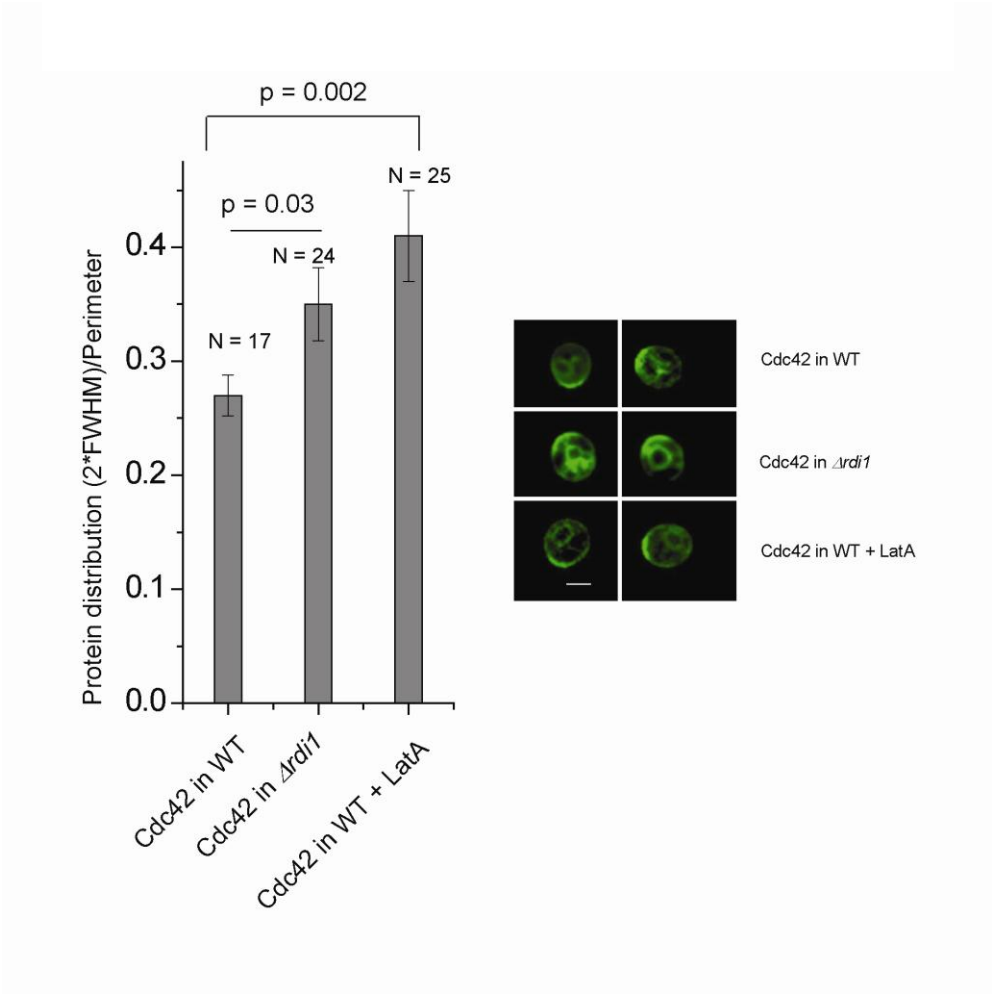

Supplemental Figure 4, related to Figures 1 and 3.

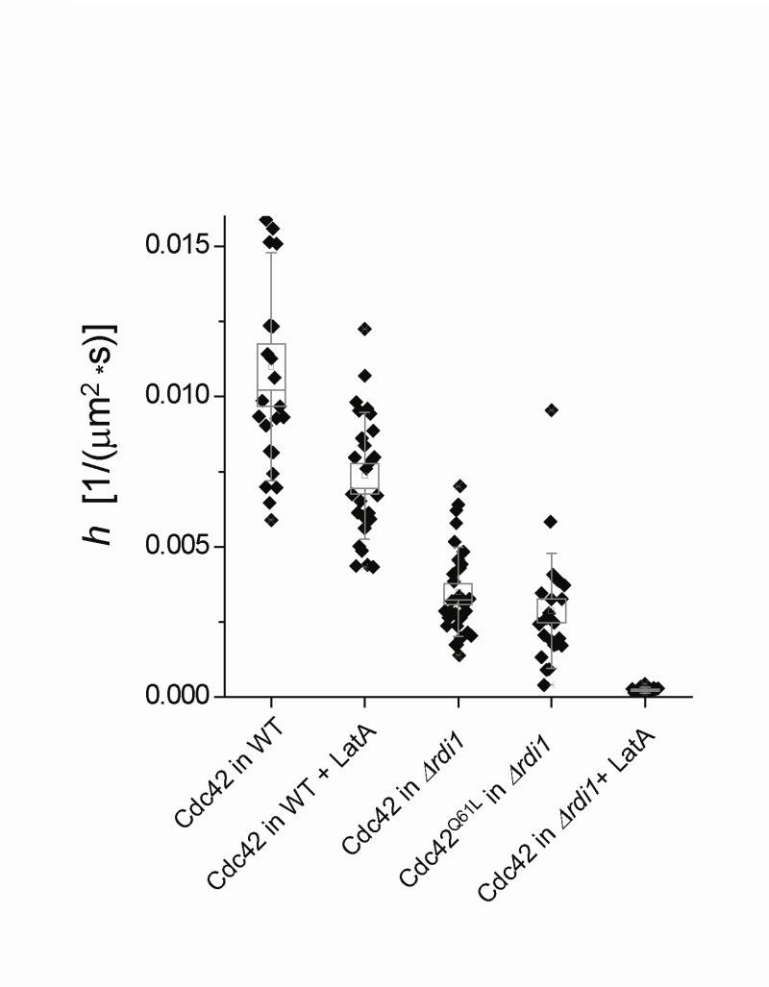

Supplemental Figure 5, related to Figure 6.

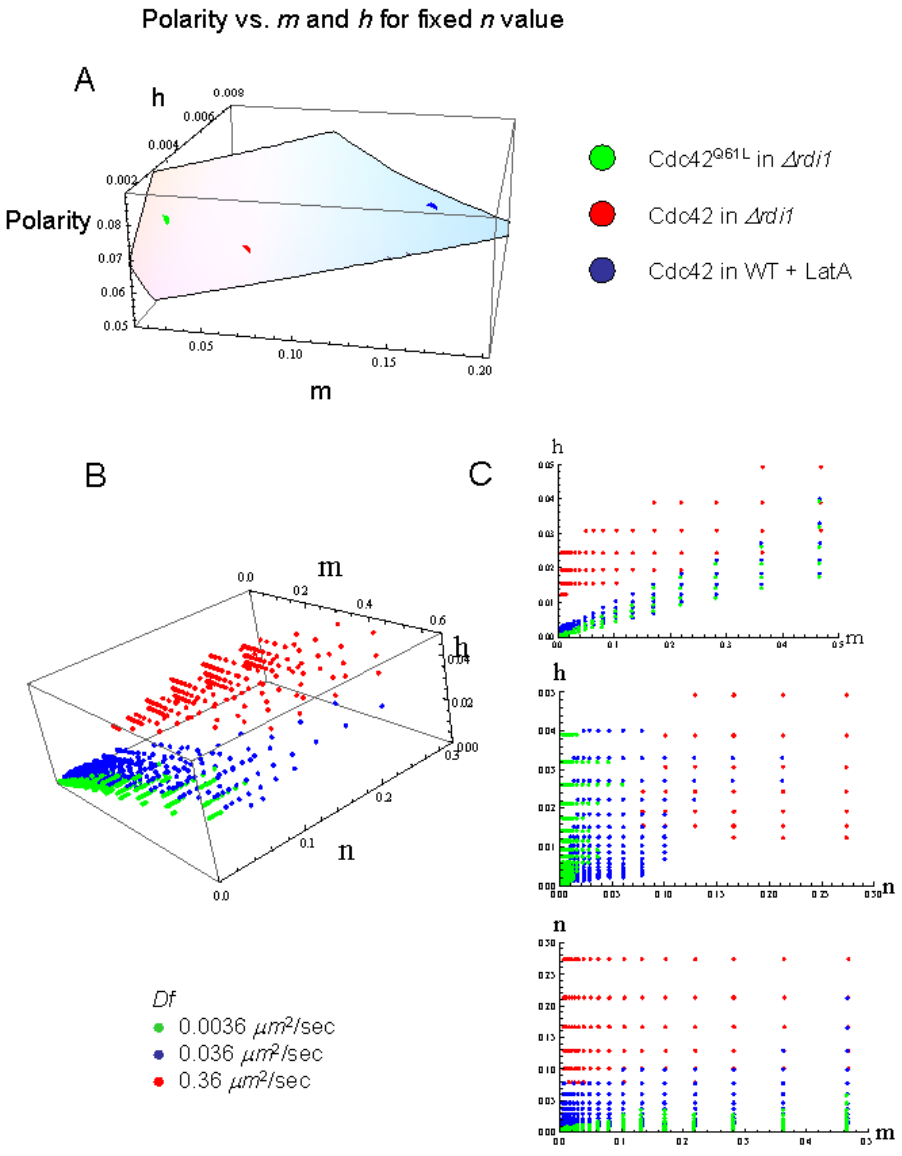

Supplemental Figure 6, related to Figure 7.

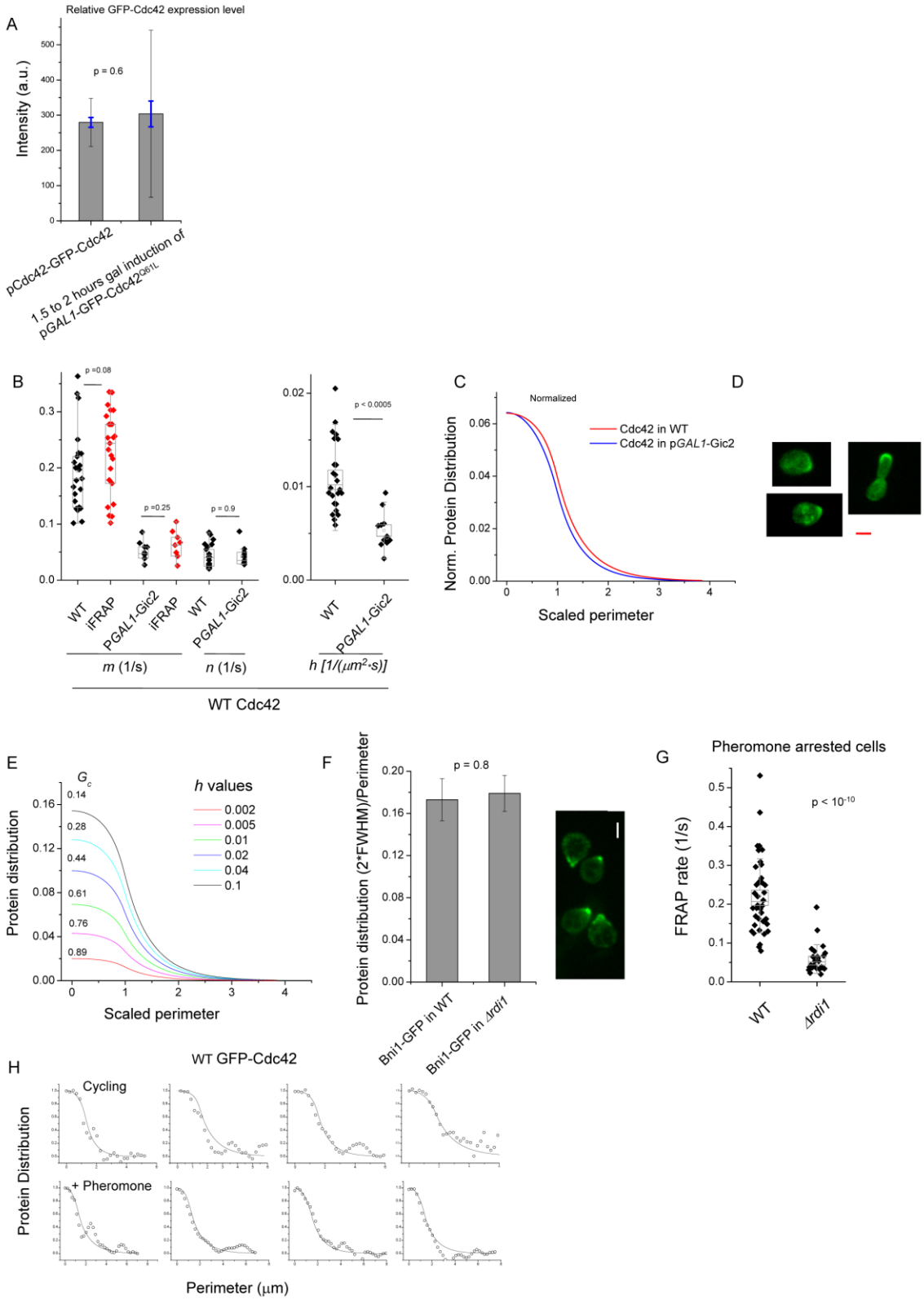

Supplemental Figure 7, related to Figure 2 and Supplemental Text.

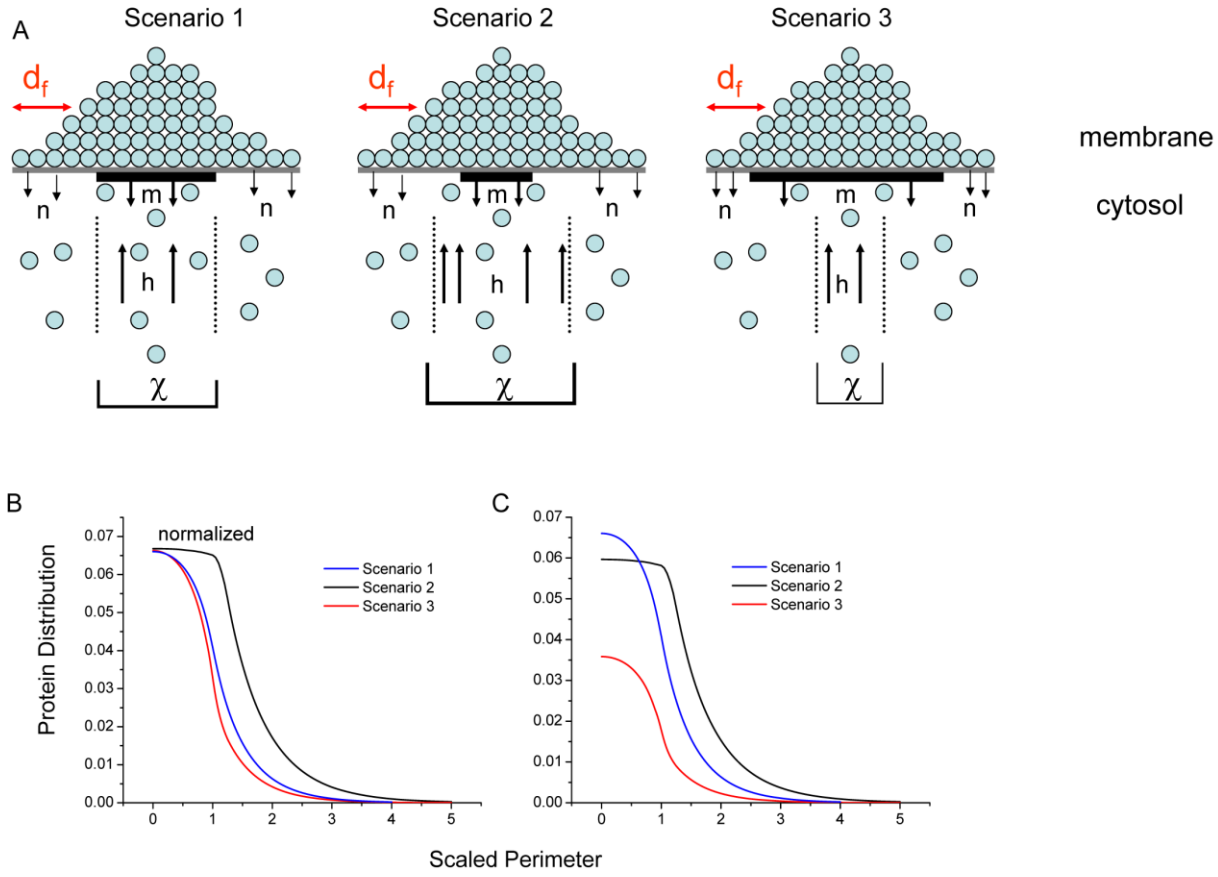

Supplemental Table 1. Yeast strains used in this study.

| RLY number | Genotype | Source |
|---|---|---|
| 2530 | *MAT*a *his3Δ1;leu2Δ0;met15Δ0;ura3Δ0* | Huh et al., 2003 |
| 2544 | *MAT*a; *RGA1-GFP::HIS5 his3Δ1;leu2Δ0;met15Δ0;ura3Δ0* | Huh et al., 2003 |
| 2667 | *MAT*a *BAT2-GFP-mCHERRY::URA3* (6AA linker) *his3Δ1;leu2Δ0;met15Δ0;ura3Δ0* | Slaughter, et al. 2007 |
| 2902 | *MAT*a; pRL369 (p*CDC42-GFP*-myc6-*CDC42* / pRS306 *URA3*) *his3Δ1;leu2Δ0;met15Δ0;ura3Δ0* | Wedlich-Soldner et al., 2004 |
| 3090 | *MAT*a; *BEM3-GFP::HIS5 his3Δ1;leu2Δ0;met15Δ0;ura3Δ0* | Huh et al., 2003 |
| 3238 | *MAT*a; *BEM2-GFP::HIS5 his3Δ1;leu2Δ0;met15Δ0;ura3Δ0* | Huh et al., 2003 |
| 3271 | *MAT*a; *ste50Δ::KAN; STE11-GFP::URA3 his3Δ1;leu2Δ0;met15Δ0;ura3Δ0* *MAT*a *bzz1Δ::GFP:HIS5* bat2Δ::m*CHERRY::URA3* | This study |
| 3291 | *his3Δ1;leu2Δ0;met15Δ0;ura3Δ0* *MAT*a; p*GAL1-GFP*-myc6-*CDC42*$^{Q61L}$ *CEN URA3* | This study |
| 3366 | *his3Δ1;leu2Δ0;met15Δ0;ura3Δ0* *MAT*a; p*GAL1-GFP*-myc6-*CDC42*$^{D57Y}$ *CEN URA3* | Wedlich-Soldner et al., 2004 |
| 3368 | *his3Δ1;leu2Δ0;met15Δ0;ura3Δ0* *MAT*a; p*GAL1-GFP*-myc6-*CDC42*$^{R66E}$ *CEN URA3* | Wedlich-Soldner et al., 2004 |
| 3425 | *his3Δ1;leu2Δ0;met15Δ0;ura3Δ0* *MAT*a; *Δrdi::LEU2* pRL369 (p*CDC42-GFP*-myc6-*CDC42* / pRS306 *URA3*) | This study |
| 3488 | *his3Δ1;leu2Δ0;met15Δ0;ura3Δ0* *MAT*a; p*GAL1-GFP*-myc6-*CDC42*$^{D57Y}$ *CEN URA3 RDI1-mCHERRY::HIS5* | This study |
| 3503 | *his3Δ1;leu2Δ0;met15Δ0;ura3Δ0* *MAT*a; p*GAL1-GFP*-myc6-*CDC42*$^{Q61L}$ *CEN URA3 RDI1-mCHERRY::HIS5* | This study |
| 3550 | *his3Δ1;leu2Δ0;met15Δ0;ura3Δ0* *MAT*a; p*GAL1-GFP*-myc6-*CDC42*$^{C188S}$ *CEN URA3 RDI1-mCHERRY::HIS5* | This study |
| 3557 | *his3Δ1;leu2Δ0;met15Δ0;ura3Δ0* | This study |
| 3559 | *MAT*a; *Δrdi::LEU2 his3Δ1;leu2Δ0;met15Δ0;ura3Δ0* | This study |
| 3619 | *MAT*a; *CDC24-GFP::HIS5 his3Δ1;leu2Δ0;met15Δ0;ura3Δ0* *MAT*a; *BNI1-GFP::HIS5 ARC40-mCHERRY::URA3* | Huh et al., 2003 |
| 3748 | *his3Δ1;leu2Δ0;met15Δ0;ura3Δ0* *MAT*a ; pRL369 (p*CDC42-GFP*-myc6-*CDC42* / prs306 *URA3*) *BNI1-* | This study |
| 3759 | *mCHERRY::HIS5 his3Δ1;leu2Δ0;met15Δ0;ura3Δ0* *MAT*a; *BNI1-GFP::HIS5 BEM2-mCHERRY::URA3* | This study |
| 3812 | *his3Δ1;leu2Δ0;met15Δ0;ura3Δ0* *MAT*a ; *Δrdi::LEU2* p*GAL1-GFP*-myc6-*CDC42*$^{D57Y}$ *CEN URA3* | This study |
| 3884 | *his3Δ1;leu2Δ0;met15Δ0;ura3Δ0* *MAT*a ; *Δrdi::LEU2* p*GAL1-GFP*-myc6-*CDC42*$^{Q61L}$ *CEN URA3* | This study |
| 3885 | *his3Δ1;leu2Δ0;met15Δ0;ura3Δ0* *MAT*a ; *BEM3-GFP::HIS5 BEM2-mCHERRY::URA3* | This study |
| 3901 | *his3Δ1;leu2Δ0;met15Δ0;ura3Δ0* *MAT*a; *Δbem2::*KAN *Δbem3*::*mCHERRY*::*HIS5* p*GAL1-GFP*-myc6-*CDC42* | This study |
| 3908 | *CEN URA his3Δ1;leu2Δ0;met15Δ0;ura3Δ0* | This study |
| 4025 | *MAT*a; *Δarp3::HIS5 PDW25 (arp3-2ts :: LEU2)* pGAL1-*GFP*-myc6-*CDC42-* R*66E CEN URA his3Δ200;leu2–3;lys2-801,ura3-52* | Winter et al., 1997 *(arp3-2)* |
| 4045 | *MAT*a; *Δarp3::HIS5 PDW25 (arp3-2ts in LEU2)* p*GAL1-GFP*-myc6-*CDC42* *CEN URA his3Δ200;leu2–3;lys2-801;ura3-52* | Winter et al., 1997 *(arp3-2)* |
| 4095 | *MAT*a ; *Δrdi::LEU2 BNI1-GFP::HIS5 his3Δ1;leu2Δ0;met15Δ0;ura3Δ0* | This study |
| 4096 | *MAT*a; p*GAL1*-myc6-*GFP-CDC42*$^{Q61L}$ *CEN URA3 BNI1-mCHERRY::HIS5* *his3Δ1;leu2Δ0;met15Δ0;ura3Δ0* | This study |
| 4308 | *MAT*a; pRL369 (p*CDC42-GFP*-myc6-*CDC42* / pRS306 *URA3*) *RDI1-* *mCHERRY::HIS5 his3Δ1;leu2Δ0;met15Δ0;ura3Δ0* | This study |

| | | |
|---|---|---|
| 4358 | *MAT*a; pRL369 (p*CDC42-GFP*-myc6-*CDC42* / pRS306 *URA3*) *RDI1-mCHERRY::HIS5 pGAL1-Gic2 CEN LEU2 his3Δ1;leu2Δ0;met15Δ0;ura3Δ0* | This study |
| 4368 | *MAT*a; *Δrdi::LEU2 BNI1-GFP::HIS5 BEM2-mCHERRY::URA3 his3Δ1;leu2Δ0;met15Δ0;ura3Δ0* | This study |
| 4404 | *MAT*a; pRL369 (p*CDC42-GFP*-myc6-*CDC42*$^{R66E}$ / pRS306 *URA3*) *RDI1-mCHERRY::HIS5 his3Δ1;leu2Δ0;met15Δ0;ura3Δ0* | This study |
| 4409 | *MAT*a; p*GAL1-GFP*-myc6-*CDC42*$^{Q61L,T35A}$ *CEN URA3 his3Δ1;leu2Δ0;met15Δ0;ura3Δ0* | This study |
| 4425 | *MAT*a; *Δrdi::LEU2* p*GAL1-GFP*-myc6-*CDC42*$^{Q61L,T35A}$ *CEN URA3 his3Δ1;leu2Δ0;met15Δ0;ura3Δ0* | This study |
| 4426 | *MAT*a; p*GAL1-GFP*-myc6-*CDC42*$^{D57Y,T35A}$ *CEN URA3 his3Δ1;leu2Δ0;met15Δ0;ura3Δ0* | This study |
| 4427 | *MAT*a; *Δrdi::LEU2* p*GAL1-GFP*-myc6-*CDC42*$^{D57Y,T35A}$ *CEN URA3 his3Δ1;leu2Δ0;met15Δ0;ura3Δ0* | This study |

## 1 Description of the model

### 1.1 Basic model

Consider a model of Cdc42 protein dynamics on the surface of a polarized yeast cell. The previous model (Marco et al., 2007) discussed the simplest case of one circular transport window on the cell surface. This model can be written in plane geometry in a form:

$$\frac{\partial f}{\partial t} = D\Delta f - m\chi f - n(1-\chi) f + h\chi F_c, \qquad \text{(S1)}$$

where $f(r,\phi,t)$ denotes the surface (membrane) density of Cdc42 protein, $D$ is the membrane diffusion coefficient, $m$ and $n$ are the internalization (protein removal) rate inside and outside the transport window, respectively. The restoration transfer rate inside the window is denoted by $h$, and $F_c$ is the cytoplasmic (intracellular) total amount of the protein. The spatially dependent function $\chi$ is equal to 1 inside the transport window, and is zero outside it. The Laplacian in the polar coordinates $\{r,\phi\}$ reads

$$\Delta f = \frac{1}{r}\frac{\partial}{\partial r}\left(r\frac{\partial f}{\partial r}\right) + \frac{1}{r^2}\frac{\partial^2 f}{\partial \phi^2}.$$

The total amount $F_{total}$ of the protein in the cell remains constant

$$F_{total} = F_c + \int_S drf(r,t) = F_c + F = const. \qquad \text{(S2)}$$

The dimensions of the parameters are:

$$[f] = 1/\mu m^2, [D] = \mu m^2/s, [m] = [n] = 1/s, [h] = 1/\mu m^2 \cdot s, [F_c] = [\chi] = 1.$$

It should be emphasized that we apply the equation (S1) for description of a polarized protein experiencing dynamic equilibrium at steady state, not during initial stages of polarity establishment.

### 1.2 Non-dimensional version

It is helpful to make the model equation non-dimensional. To perform this task we introduce the following scales:

- Protein amount scale $F_{total}$ (total protein amount)
- Length scale $r_0$ (characteristic window size)
- Time scale $t_0 = r_0^2/D$

Using these scales we have a set of new variables we can define as follows:

$$\tau = t/t_0, u = r/r_0, G_c = F_c/F_{total}, g = fr_0^2/F_{total}.$$

Substituting these relations into the equations (1) and (2) we have

$$\frac{\partial g}{\partial \tau} = \Delta g - M^2 \chi g - N^2(1-\chi)g + \chi B, \quad \text{(S3)}$$

where $M^2 = mr_0^2/D, N^2 = nr_0^2/D, B = \gamma G_c, \gamma = hr_0^4/D$. The conservation condition (S2) reads

$$G_c + \int_S dug(u,\tau) = G_c + G_m = 1. \quad \text{(S4)}$$

As the yeast cell shape can be approximated by a sphere, we need to justify the replacement of the spherical geometry by the plane geometry. We performed a comparison of numerical solutions of the problem (S3) in both coordinate systems. The computation showed that the obtained distributions are very close one to the other (not shown). Taking into account the noise of the experimental data, we conclude that usage of the plane geometry model is justified.

## 2 Steady state solution

As we are examining the relationship of dynamic parameters that lead to the observed distribution of Cdc42 at steady state and not at intial polarity establishment, we restrict ourself to computation of the steady state solution $g(u)$ satisfying the equation:

$$\Delta g - M^2 \chi g - N^2(1-\chi)g + \chi B = 0. \quad \text{(S5)}$$

### 2.1 One window, one pathway

Assuming the radial symmetry of the problem we rewrite equation (S5) as a set of two equations in two regions - region 1 (inside the transport circular window) and region 2 (outside it) [see Fig.2 in main text]. As we choose the radius of the window to be a length scale $r_0$, the nondimensional window size is equal to one. The solutions in each region are marked by corresponding subscript.

$$\Delta g_1 - M^2 g_1 + B = 0, \quad \text{(S6)}$$

$$\Delta g_2 - N^2 g_2 = 0, \tag{S7}$$

where

$$\Delta g_i = \frac{1}{u}\frac{d}{du}\left(u\frac{dg_i}{du}\right) = g_{i''}(u) + \frac{1}{u}g'_i(u).$$

The functions $g_i(u)$ satisfy the following boundary conditions (BC)

$$g'_1(0) = 0,\ \ g_1(1) = G,\ g_2(1) = G, \lim_{u\to\infty} g_2(u) = 0. \tag{S8}$$

The first condition means that there is no flux of protein at the center of the window, the last BC requires that the membrane protein density vanishes far from the window. The two other conditions say that the solutions on both sides of the window boundary should be equal one to the other and to some (undefined) value $G$. This value is found from the additional matching condition at $u = 1$ which requires that also the first derivatives of the solutions should be equal on both sides of the window boundary:

$$g'_1(1) = g'_2(1). \tag{S9}$$

The solution of the equation (S6,S7) reads

$$g_1(u) = \frac{B}{M^2} + \left(G - \frac{B}{M^2}\right)\frac{I_0(Mu)}{I_0(M)}, \tag{S10}$$

$$g_2(u) = G\frac{K_0(Nu)}{K_0(N)}, \tag{S11}$$

where $I_k(u)$ and $K_k(u)$ denote the modified Bessel functions of the first and second kind, respectively. Substitution of these solutions into the matching condition (S9) leads to the relation

$$\left(G - \frac{B}{M^2}\right)\frac{MI_1(M)}{I_0(M)} = -G\frac{NK_1(N)}{K_0(N)},$$

from which the value of $G$ is found as

$$G = \frac{B}{M^2}P(M,N),\quad P(M,N) = \frac{MI_1(M)}{I_0(M)}\left[\frac{MI_1(M)}{I_0(M)} + \frac{NK_1(N)}{K_0(N)}\right]^{-1}. \tag{S12}$$

Thus the formulae (S10,S11) and (S12) completely desribe the radial distribution of the membrane protein.

It is worth mentioning that the above method of solution also enables us to find the relative amount of cytoplasmic protein in the steady state regime (note that in the previous work

both membrane distribution and cytoplasmic protein amount were computed as a solution of the time dependent problem). To compute $G_c$ we find the total amount $G_m$ of the membrane protein by integrating the solutions in the respective regions

$$G_m = 2\pi\left(\int_0^1 u g_1(u)du + \int_1^\infty u g_2(u)du\right) = 2\pi\frac{\gamma G_c}{M^2}\left[\frac{1}{2} + (P-1)\frac{I_1(M)}{MI_0(M)} + P\frac{K_1(N)}{NK_0(N)}\right]. \quad \text{(S13)}$$

Now using the condition (S4) we obtain

$$G_c + 2\pi\frac{\gamma G_c}{M^2}\left[\frac{1}{2} + (P-1)\frac{I_1(M)}{MI_0(M)} + P\frac{K_1(N)}{NK_0(N)}\right] = 1, \quad \text{(S14)}$$

from which the value of $G_c$ is computed easily. Comparing the computed value to that of experiment, one can verify the validity of the suggested model on a cell by cell basis (main text, Fig.3).

### 2.2 One window, two pathways

Consider a slight extension of the above problem assuming that there exist two independent pathways with different transfer rates acting inside the same window (see Fig. 2, main text). Denote the transfer rates of $i$-th ($i = 1,2$) process with distribution $g_i$ as $M_i, N_i$ and $h_i$. The equation (S5) is changed into the set of two equations for $g_i$:

$$\Delta g_1 - M_1^2\chi g - N_1^2(1-\chi)g + \chi\gamma_1 G_c = 0, \quad \text{(S15)}$$

$$\Delta g_2 - M_2^2\chi g - N_2^2(1-\chi)g + \chi\gamma_2 G_c = 0, \quad \text{(S16)}$$

where $g = g_1 + g_2$. It is easy to see that this system leads to (S5), so that its solution is given by formulae (S10,S11) and (S12) with

$$M^2 = M_1^2 + M_2^2,\ N^2 = N_1^2 + N_2^2,\ B = (\gamma_1 + \gamma_2)G_c = \gamma G_c. \quad \text{(S17)}$$

### 2.3 Two concentric windows, two pathways

The next extension of the basic model leads to the consideration where there are two concentric windows of the (normalized) radii $u_0 < 1$ and 1. This case is described by the following system where $\chi_i$ is equal to 1 inside the $i$-th process window and 0 outside.

$$\Delta g_1 - M_1^2 \chi_1 g - N_1^2 (1-\chi_1) g + \chi_1 \gamma_1 G_c = 0, \tag{S18}$$

$$\Delta g_2 - M_2^2 \chi_2 g - N_2^2 (1-\chi_2) g + \chi_2 \gamma_2 G_c = 0, \tag{S19}$$

We can assume without loss of generality that in the smaller window of radius $u_0$ both pathways are employed, while in the ring $u_0 \le u \le 1$ only the second pathway ($i = 2$) survives. Thus we consider a problem in three regions: the first one is the inner circle ($0 \le u \le u_0$), the second region coincides with the outer ring ($u_0 \le u \le 1$), and the third one is outside of the larger circle ($1 \le u$) (see Fig. 2, main text). Writing down the equations in each region we arrive at the system:

$$\Delta g_1 - (M_1^2 + M_2^2) g_1 + (\gamma_1 + \gamma_2) G_c = 0, \tag{S20}$$

$$\Delta g_2 - (M_2^2 + N_1^2) g_2 + \gamma_2 G_c = 0, \tag{S21}$$

$$\Delta g_3 - (N_1^2 + N_2^2) g_3 = 0, \tag{S22}$$

subject to the following BC

$$g'_1(0) = 0,\ g_1(u_0) = g_2(u_0) = G_1,\ g_2(1) = g_3(1) = G_2,\ \lim_{u\to\infty} g_3(u) = 0.$$

The values $G_1$ and $G_2$ are determined from two matching conditions

$$g'_1(u_0) = g'_2(u_0),\ \ g'_2(1) = g'_3(1).$$

The solution of equation (S20) reads

$$g_1(u) = \frac{B}{M^2} + \left( G_1 - \frac{B}{M^2} \right) \frac{I_0(Mu)}{I_0(Mu_0)} \tag{S23}$$

with parameters given by (S17). It is easy to show that in the region 2 the solution can be presented as

$$g_2(u) = \frac{B}{M^2} + C_1 I_0(Mu) + C_2 K_0(Mu), \tag{S24}$$

where

$$M^2 = M_2^2 + N_1^2, B = \gamma_2 G_c. \quad \text{(S25)}$$

and the integration constants $C_1, C_2$ are obtained from the conditions

$$\frac{B}{M^2} + C_1 I_0(Mu_0) + C_2 K_0(Mu_0) = G_1, \ \frac{B}{M^2} + C_1 I_0(M) + C_2 K_0(M) = G_2.$$

The explicit expressions for the constants are cumbersome and are not presented here but are available upon request. Finally, the solution in the outer region is similar to (S11)

$$g_3(u) = G_2 \frac{K_0(Nu)}{K_0(N)}. \quad \text{(S26)}$$

Using the matching conditions we determine the values $G_1$ and $G_2$. Then the total membrane protein amount is computed as

$$G_m = 2\pi\left(\int_0^{u_0} u g_1(u)du + \int_{u_0}^{1} u g_2(u)du + \int_1^{\infty} u g_3(u)du\right). \quad \text{(S27)}$$

Substitution of the obtained expression into the conservation relation $G_m + G_c = 1$ gives us the total intracellular protein $G_c$.

### 2.4 Two concentric windows, one pathway

It is also possible to use the subset of equations (S20-S22) to consider the possibility of a single recycling mechanism in the case when the return flow area is not equal to the window of internalization. When the return flow area is larger in size than the window of internalization we use the following set of parameters in equations (S20-S22)

$$M_1 = 0, \ M_2 = M, \ N_1 = 0, \ N_2 = N, \ \gamma_1 = \gamma, \ \gamma_2 = 0,$$

and when the return flow area is smaller in size than the window of internalization we use the following set

$$M_1 = M, \ M_2 = 0, \ N_1 = N, \ N_2 = 0, \ \gamma_1 = 0, \ \gamma_2 = \gamma.$$

Supplemental Fig. 7 shows the characteristic effect on the distribution for theoretical values in both these cases. While the model can in general be applied to these cases, we limit our experimental examination of Cdc42 dynamics to the possibilities outlined in subsections 2.1, 2.2, and 2.3.

### 2.5 No window (uniform membrane distribution)

Consider a degenerate case of uniformly distributed membrane protein. It is described by the equation

$$-M^2 g + \gamma G_c = 0, \tag{S28}$$

where $g$ is the uniform protein density. Denoting the membrane surface area by $S$ we obtain $G_m = Sg$ and find $G_c = 1 - G_m = 1 - Sg$. Thus, the membrane steady-state density $g$ satisfies the equation $M^2 g = \gamma(1 - Sg)$ and we find

$$g = \frac{\gamma}{M^2 + \gamma S}. \tag{S29}$$

## 3 Parameters estimate

The dimensional parameters required for the solution of the problem and calculation of the Cdc42 steady state membrane distribution are the diffusion coefficient $D$, internalization rates $m$, inside, and $n$, outside, of the transport window, and the membrane protein restoration rate $h$. All parameters except the diffusion coefficient are found from the combination of FRAP and steady-state imaging experiments as described below. The value of $D$ of $0.036$ $\mu m^2/s$ is used as published (Marco et al., 2007). As the FRAP process is essentially non-stationary we use equation (S1) as a starting point and use time dependent FRAP data along with imaging to determine model parameters, which are converted into nondimensional units and used to calculate the steady state distributions.

### 3.1 Computation of model parameters

Integrating the local membrane protein density $f(r,t)$ over the membrane surface we obtain the total membrane protein $F(t) = \int_S drf(r,t)$ as a function of time. Similarily we find the total amount $W(t)$ inside the window $W(t) = \int_w drf(r,t)$.

With the premise that the Cdc42 distribution is controlled by a flux balance characterized by equation (S1) and that local surface diffusion does not affect the total amount of membrane protein $F(t)$, then after integration of (S1) the following must be true

$$F'(t) = -mW - n(F - W) + hAF_c, \tag{S30}$$

$$F_{total} = F_c + F, \tag{S31}$$

where $A$ is the window area. Note that we do not have an independent equation describing the dynamics of $W$.

As the bleaching is applied to the surface only (mainly in the region of the transport window) the dynamics of both $F$ and $W$ are described by exponential saturation

$$F(t) = F_0 + F_1(1 - e^{-\alpha t}), W(t) = W_0 + W_1(1 - e^{-\beta t}). \tag{S32}$$

From the conservation of the total cell protein (S31) it follows that

$$F_c(t) = F_{total} - F(t) = F_{total} - F_0 - F_1(1 - e^{-\alpha t}).$$

We estimate the values $F_{total}, F_0, F_1, W_0, W_1, \alpha$ and $\beta$ from the experimental data, by simple extraction from independent, single exponential fits to $F(t)$ and $W(t)$ (Supplemental Fig. 2B). Substituting (S32) with the estimated values into (S30) we obtain the condition for the determination of the parameters $m, n, h$ (using a linear regression method)

$$\alpha F_1 e^{-\alpha t} = AhF_{total} - (n + Ah)[F_0 + F_1(1 - e^{-\alpha t})] - (m - n)[W_0 + W_1(1 - e^{-\beta t})], \tag{S33}$$

obtained for time moments $t$.

From simple algebraic rearrangements of (S33) it is possible to obtain several conditions on the parameter values. Consider first a possibility when $\alpha \neq \beta$. As the condition (S33) must hold for any time $t$, rearrangements and grouping of time-dependent and time-independent terms in (S33) implies the following relations

$$\alpha = n + Ah, \quad AhF_{total} - \alpha(F_0 + F_1) = 0, \quad m = n.$$

The last equality corresponds to a particular case when the internalization rates inside and outside the window are equal. While this is certainly possible, there is no justification for limiting our consideration to this scenario. To the contrary, ample evidence exists to suggest that endocytic machinery is highly polarized, and thus at least for endocytic internalization, we anticipate $m > n$.

Therefore, in the general case, to consider $m \neq n$, it is nesessary that $\alpha = \beta$ and we obtain two conditions

$$AhF_{total} - (n + Ah)(F_0 + F_1) - (m - n)(W_0 + W_1) = 0, \quad \alpha F_1 = (n + Ah)F_1 + (m - n)W_1. \qquad \text{(S34)}$$

With 3 unknowns and 2 conditions at this point we cannot yet compute all three parameters $m, n$ and $h$, and we need a third condition. For a given value of $m/n$ ratio we find the parameters $m, n$ and $h$; then compute the nondimensional values $M, N$ and $\gamma$. We find the distributions $g_1(u)$ for the window region and $g_2(u)$ for the outside region, and compare the experimentally measured ratio $W/F$ of window to total membrane fluorescence to the following calculation:

$$\frac{W}{F} = \frac{G_w F_{total}}{G_m F_{total}} = \frac{G_w}{G_m} = \frac{\int_0^1 u g_1(u) du}{\int_0^1 u g_1(u) du + \int_1^\infty u g_2(u) du}. \qquad \text{(S35)}$$

This equation represents the third condition, the relation between the dimensional $W, F$ and nondimensional $G_w, G_m$ quantities, where $G_m$ is defined in (S13) and $G_w$ denotes the scaled total protein inside the window. We use an iterative procedure to fit the ratio $m/n$ value to obtain the experimental value of the $W/F$ ratio known from the experimental image. This iteration allows for a unique solution of $h$, $m$, and $n$ for each cell.

In the case of a uniform membrane distribution (applied here to $\Delta rdi1+$ Lat A), the computation of model parameters is a much simplified case of the situation described above. Equation (S30) simplifies to

$$F'(t) = -mF + Ah(F_{total} - F). \qquad \text{(S36)}$$

Using $F(t) = F_0 + F_1(1 - e^{-\alpha t})$, we obtain $F' = \alpha F e^{-\alpha t}$, which leads to the modified form of equation (33)

$$\alpha F e^{-\alpha t} = AhF_{total} - (m + Ah)(F + F_0 - F_1(1 - e^{-\alpha t})). \qquad \text{(S37)}$$

Parameters, including the time constant $\alpha$, are obtained as explained above and as shown in Supplemental Fig. 2B, with the exception that there is only one region considered (there is no inside/outside window). Since equation (S37) must hold for all times $t$, we group time-dependent and time-independent terms to find the relations

$$\alpha = m + Ah, \quad AhF_{total} = \alpha(F_0 + F_1), \tag{S38}$$

from which it is follows that

$$h = \frac{\alpha(F_0 + F_1)}{AF_{total}}. \tag{S39}$$

## 4 3D correction

The functions $F$ and $W$ in the main text describe the protein amount over the total cell surface, while the measurements are made using a confocal microscope, so that only a portion of the total protein amount is detected. This means that the experimental data $F^{exp}$ should be scaled up by a coefficient $r_1$ to give the actual amount $F = r_1 F^{exp}, W = r_1 W^{exp}$. The same reasoning is applied to the computation of the cytosol actual value of $F_c = r_2 F_c^{exp} = r_2 (F_{total}^{exp} - F^{exp})$.

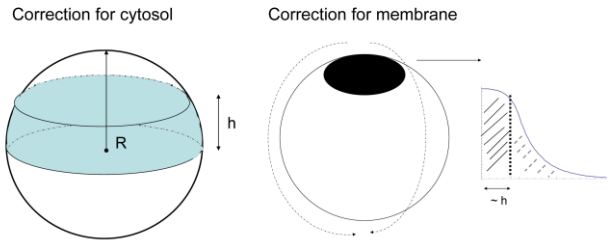


The above pictures describe the computation of $r_2$ (left) and $r_1$ (right) correction coefficient respectively.

As the cytosol protein distribution is assumed to be uniform, one can compute $r_2$ as a ratio of volume $V_R = 2\pi R^3/3$ of a semisphere of radius $R$ to the volume $V_h = \pi h(3R^2 - h^2)/3$ of the spherical slice of the height $h < R$ (where $2h$ is the width of the confocal slice)

$$r_2 = V_R/V_h = \frac{2}{\delta(3 - \delta^2)}; \ \delta = h/R.$$

The value of $2h = 1.5\,\mu$m for our system was found from a $z$-stack series of sub-diffraction beads. Comparison of $h$ to $R$ gives the value of $r_2 = 1.66$ for the cytosol.

Assuming for simplicity that the membrane protein is distributed evenly over the surface, and noting that the thickness of the confocal slice $h \approx 0.4R$ we find an estimate for maximum $r_1 = R/h \approx 2.5$. The actual value must be lower, as Cdc42 is polarized. For a spherical cell that is symmetric around the polar cap, a linescan, starting at the cap center, around the perimeter in any orientation represents the membrane distribution. We fit a linescan around the perimeter of our cells, as in the orientation shown in Fig. 4B, and integrated the region that corresponds to inside the center confocal slice, based on our knowledge of the size of our confocal slice. The ratio of this integral to the integral of the total linescan is a very close approximation of the relative amount of membrane Cdc42 inside the center confocal slice.

**Analysis of the parameter space of Cdc42 dynamics**

To explore the relationship of all model parameters to polarity in general, we searched parameter space for combinations of *m, n,* and *h* that would satisfy specified requirements for a polarized system at three values of $D_f$: 0.36, 0.036, and 0.0036 $\mu m^2$/sec. The criteria that we specified for the observed polarized system included $G_c$ values within the experimentally observed range (45 to 70%), and Cdc42 relative abundance in the delivery window from 12 to 30% of the total. As a third criterion, polarity was confined to the range observed experimentally. The three-dimensional parameter-space plot is shown in Supplemental Fig. 5B, while projections are shown in Supplemental Fig. 5C. For $D_f$ values that are either as observed for prenylated proteins in yeast (0.036 $\mu m^2$/sec) (Marco et al., 2007) or 10 fold slower, the allowable ranges of *m, n,* and *h* were clustered. Allowable values of internalization rate inside the window (*m)* and rate of delivery (*h*) at slow membrane diffusion rates reside in a linear range: for a given $D_f$ and *n*, an increase in *m* can be balanced by an increase in *h*. For a polarized system, this simply suggests that if internalization rate is increased, the system can remain polarized by an increased rate of delivery. In fact, we observe this experimentally for $Cdc42^{Q61L}$ in *Δrdi1*, WT Cdc42 in *Δrdi1*, and WT Cdc42 + LatA. In these three cases, while *n* is similar, *m* and *h* vary. However, the ratio of *h/m* is within 3 fold of each other, and in fact the difference in the ratio of *h/m* in these cases explains the differences in polarity observed in main text Fig. 7A. However, at a membrane diffusion rate 10 fold higher than that observed for Cdc42, the relationship between

internalization rate inside the window (*m)* and rate of delivery (*h)* is not as limited, as *h* must be higher to balance also the increased rate of diffusion away from the site of deposition.

In contrast, a linear relationship is not observed between rate of delivery (*h)* and internalization rate outside the window *(n),* or between *n* and *m.* Instead, box-like ranges of allowed values are observed. In addition, at low diffusion rates, for fixed *m*, or fixed *h*, a small range of *n* values are allowed. This suggest that if *n* represents a basal internalization rate of Cdc42 outside the delivery window, its allowable values are mostly independent of *h* and *m* but instead are more constrained by the rate of membrane diffusion.

With the acknowledgement that the criteria here are set up using observed parameters of Cdc42 polarization and are only applicable for a system of size and shape similar to yeast, it is still interesting to observe the differences in parameter values needed to satisfy a polarized system in the case of rapid membrane diffusion. This is notable because, while a value of 0.036 $\mu m^2$/sec has been measured for the prenylated protein Cdc42 (Marco et al., 2007) and 0.0036 $\mu m^2$/sec is in line with diffusion of transmembrane proteins in yeast (Ries and Schwille, 2006; Valdez-Taubas and Pelham, 2003), membrane diffusion in mammalian system is predicted to be much faster (Ries et al., 2009; Semrau and Schmidt, 2007). The parameter space analysis here suggests that in order to maintain a polarized state based on these criteria in the presence of more rapid membrane diffusion, vastly different dynamic parameters are needed.

**Supplemental References:**

Huh, W.K., Falvo, J.V., Gerke, L.C., Carroll, A.S., Howson, R.W., Weissman, J.S., and O'Shea, E.K. (2003). Global analysis of protein localization in budding yeast. Nature *425*, 686-691.

Marco, E., Wedlich-Soldner, R., Li, R., Altschuler, S.J., and Wu, L.F. (2007). Endocytosis optimizes the dynamic localization of membrane proteins that regulate cortical polarity. Cell *129*, 411-422.

Rancati, G., Pavelka, N., Fleharty, B., Noll, A., Trimble, R., Walton, K., Perera, A., Staehling-Hampton, K., Seidel, C.W., and Li, R. (2008). Aneuploidy underlies rapid adaptive evolution of yeast cells deprived of a conserved cytokinesis motor. Cell *135*, 879-893.

Ries, J., Chiantia, S., and Schwille, P. (2009). Accurate determination of membrane dynamics with line-scan FCS. Biophys J *96*, 1999-2008.

Ries, J., and Schwille, P. (2006). Studying slow membrane dynamics with continuous wave scanning fluorescence correlation spectroscopy. Biophys J *91*, 1915-1924.

Semrau, S., and Schmidt, T. (2007). Particle image correlation spectroscopy (PICS): retrieving nanometer-scale correlations from high-density single-molecule position data. Biophys J *92*, 613-621.

Slaughter, B.D., Schwartz, J.W., and Li, R. (2007). Mapping dynamic protein interactions in MAP kinase signaling using live-cell fluorescence fluctuation spectroscopy and imaging. Proc Natl Acad Sci USA *104*, 20320-20325.

Valdez-Taubas, J., and Pelham, H.R. (2003). Slow diffusion of proteins in the yeast plasma membrane allows polarity to be maintained by endocytic cycling. Curr Biol *13*, 1636-1640.

Wedlich-Soldner, R., Wai, S.C., Schmidt, T., and Li, R. (2004). Robust cell polarity is a dynamic state established by coupling transport and GTPase signaling. J Cell Biol *166*, 889-900.

Winter, D., Podtelejnikov, A.V., Mann, M., and Li, R. (1997). The complex containing actin-related proteins Arp2 and Arp3 is required for the motility and integrity of yeast actin patches. Curr Biol *7*, 519-529.

**Supplemental Figure 1**. **A**. Representative images of budding cells expressing GFP-Cdc42 in the *Δrdi1* background, cells in the WT background after treatment with 100 μM LatA, and cells in the *Δrdi1* background treated with LatA. Scale bar is 2.0 μm. Removal of one of the two pathways does not result in loss of polarization, but removal of both pathways results in loss of polarity. **B**. FRAP rates of Cdc42 in WT, Cdc42 in WT + LatA, Cdc42 in *Δrdi1*, and the sum of all possible combinations of the rate of FRAP for Cdc42 in WT treated LatA, and Cdc42 in *Δrdi1*. Box width is the standard error of the mean, whiskers represent the standard deviation. The rate of recovery of Cdc42 in WT is statistically indistinguishable from all combinations of summed rates of cells from the the individual pathways.

**Supplemental Figure 2. A.** Examples of overlap of Bni1-GFP and Arc40-mCherry (actin patch marker) membrane distributions. A dual-color time-series was summed, average background was subtracted, and a linescan of the cell perimeter was plotted. Black lines in the plot represent the window area, as defined in the main text. Actin patches are highly polarized inside of the window area defined by Bni1, with a sharp slope at the window edge, justifying the window modeling approach used in the text. **B**. Representation of parameters obtained from exponential fits of FRAP data. $F_0$ and $W_0$ are the initial amplitudes of the FRAP curves for the total membrane and window region, respectively, while $F_0 + F_1$ and $W_0 + W_1$ are the final amplitudes. See Experimental Procedures for information on parameter extraction from these values.

**Supplemental Figure 3**. Protein distribution as (2*FWHM)/perimeter for Cdc42 in the conditions shown. See Fig. 3 in the main text for details. A Gaussian distribution was used to for calculating FWHM. Error bars are the standard error of the mean. Representative images are shown, scale bar is 2.0 μm.

**Supplemental Figure 4.** Values of the delivery parameter *h*, from the application of the modified model assuming no transport window (or a single transport window covering the entire cell surface) to non-polarized *Δrdi1* cells treated with LatA (Cdc42 in *Δrdi1*+LatA), compared to values of *h* from the model with a polarized delivery window. See section 2.5 of Supplemental information for description of the modified model. The larger area of delivery in the case of non-polarized cells leads to a reduction in *h*.

**Supplemental Figure 5. A.** A 3-dimensional plot of polarity (peak height over width) as a function of *m* (1/s) and *h* (1/(μm$^2$*s) for a fixed value of *n* *(*0.022 (1/s)). Locations on the plot for average rate of delivery (*h)* and internalization rate inside e the window (*m)* values are shown for the conditions labeled. The plot emphasizes the general trend that polarity increases with reduction in the rate of internalization inside the delivery window (*m*). **B, C**. Parameter space analysis. A polarized system is defined as one where the total membrane protein ranges from 30 to 55% of the total, the protein in the delivery window ranges from 12 to 30% of the total, and whose peak polarity falls in the range we observe experimentally including all conditions tested. Three values of membrane diffusion were used: 0.36, 0.036, and 0.0036 $\mu m^2$/sec are represented in red, blue, and green, respectively. A three dimensional plot is shown in **B**, while projections are shown in **C**.

**Supplemental Figure 6A**. Relative expression level (in arbitrary units) of pCdc42-GFP-Cdc42 compared to p*GAL1*-GFP-Cdc42$^{Q61L}$ after 1.5 to 2 hours of *GAL* induction, measured as the integrated fluorescence signal in individual cells. Results show that this induction time does not result in significant overexpression of Cdc42 vs. expression by the endogenous promoter. Blue error bars are the standard error of the mean, black bars represent the standard deviation. **B-D**. Results of application of the model to cells expressing WT Cdc42 and p*GAL1*-Gic2 upon overexpression with galactose for 2.5 hours. **B**. Model parameters (black) and comparison to iFRAP measurements (red) are shown. Internalization rate *m* inside the window is reduced, while *n* remains unchanged. Box width is the standard error of the mean, whiskers represent the standard deviation. **C.** Reduction in *m* relative to *n* for cells overexpressing Gic2 leads to a predicted steady-state distribution that is more pointed than for WT. **D**. Example of the corresponding pointed morphology for cycling cells overexpressing Gic2. Scale bar is 2.0 μm. **E**. Theoretical curves and $G_c$ values for steady-state distributions using the *h* [1/(μm$^2$∗s)] values shown. In all cases, *m* and *n* were set to 0.19 and 0.43 1/s, respectively (the values for WT Cdc42). This plot shows that for given *m* and *n*, differences in *h* only serves to change the amplitude of the distribution and $G_c$, not the shape. **F.** Comparison of protein distribution width, calculated as shown in Fig. 3 of the main text, for Bni1-GFP in cells arrested with 75 μM mating pheromone. Representative images are shown for Bni1-GFP in *Δrdi1*. Error bars represent the standard error of the mean. Scale bar is 2.0 μm. **G**. Comparison of FRAP rates of Cdc42 in WT and *Δrdi1* backgrounds in cells arrested with 75 μM α-factor for 1 to 1.5 hours. Box width is the standard error of the mean, whiskers represent the standard deviation. **H.** Overlay of steady-state membrane Cdc42 distributions observed experimentally in individual cells and those as

calculated from model parameters extracted from imaging and FRAP data of the same cells. A linescan was drawn around half the cell perimeter. The y-axis represents the protein abundance in arbitrary units, while the x-axis represents half the perimeter (assuming symmetry) in μm. Sharper distributions were observed for Cdc42 in pheromone arrested cells, consistent with the modeling results in Fig. 7 of the main text. Dots represent the experimental values, while smooth lines represent the model-calculated distributions.

**Supplemental Figure 7**. Application of the model for the cases where the internalization window size is smaller (scenario 2) or larger (scenario 3) than the delivery window size (see section 2.4 of Supplemental Information). **B**. Theoretical effect of differing size internalization and delivery windows for arbitrary, fixed values of *m*, *n*, and *h* (assuming for theoretical purposes that the values of these parameters do not change, just the sizes of windows). A smaller area of delivery had little change on the shape of the distribution (normalized curves are shown in **B**), making it slightly more narrow, but had a large effect on the strength of the distribution (**C**). A wide delivery window relative to internalization window led to a plateau-like distribution.